Effect of Single-Slice CT Segmentation Methods on Fat Volume and Body Shape Estimation

Lilla Szatmáriné Egeresi

Division of Radiology and Imaging Science, Department of Medical Imaging, Faculty of Medicine, University of Debrecen, Nagyerdei krt. 98, 4032 Debrecen, Hungary, E-mail: egeresi.lilla@med.unideb.hu

András Székely

Kenézy Gyula Hospital, Department of Radiology, Bartók Béla út 2-26, 4031 Debrecen, Hungary, E-mail: andras.szekely@med.unideb.hu

Piroska Kallos-Balogh

Division of Nuclear Medicine and Translational Imaging, Department of Medical Imaging, Faculty of Medicine, University of Debrecen, Nagyerdei krt. 98, 4032 Debrecen, Hungary, E-mail: balogh.piroska@med.unideb.hu

Lajos Trón

Division of Nuclear Medicine and Translational Imaging, Department of Medical Imaging, Faculty of Medicine, University of Debrecen, Nagyerdei krt. 98, 4032 Debrecen, Hungary, E-mail: tron.lajos@med.unideb.hu

Ildikó Garai

Scanomed Nuclear Medicine Center, Nagyerdei krt. 98, 4032 Debrecen, Hungary, E-mail: garai.ildiko@scanomed.hu

László Balkay

Division of Nuclear Medicine and Translational Imaging, Department of Medical Imaging, Faculty of Medicine, University of Debrecen, Nagyerdei krt. 98, 4032 Debrecen, Hungary, E-mail: balkay.laszlo@med.unideb.hu

Abstract: Several automatic and semi-automatic algorithms for adipose tissue (AT) segmentation in CT have been proposed. Our study aimed to determine the effect of the preselected HU range, on the resulting AT volumes and establish whether there is a relationship between body shape and AT values determined, from a single slice. Scans of 98 patients acquired using two CT protocols, were used. Three axial slices were selected from each subject's CT data. Subcutaneous and visceral adipose tissues (SAT, VAT) were manually segmented and analyzed using three different HU ranges. In addition, a simple BMI calculation model was created by the segmented data. The areas segmented with the three different HU ranges, correlated well with each other in the case of SAT (r^2=0.99, and r^2=0.99) and VAT (r^2=0.99, and r^2=0.998). The preselected slice position had no significant effect on correlation; however, the absolute values of ATs were statistically different. CT image data acquired with higher tube current yielded a better correlation between SAT, VAT, and BMI. We also found that the correlation of VAT area to mass and BMI was weaker than the corresponding SAT correlations. The simple model-based BMI estimation is in line with real BMI data (males: r^2=0.78, females: r^2=0.841). The segmentation threshold does not substantially affect correlation, among the segmented AT values; however, their absolute values are significantly different. In addition, and interestingly, the body shape can be accurately described from the segmented AT data from a single CT slice.

Keywords: CT; fat; segmentation

1 Introduction

It is well known that obesity is closely associated with diabetes, fatty liver, cardiovascular disease and various cancers [2, 17, 24, 33]. Visceral fat resides between organs, while subcutaneous fat is located beneath the skin. Another substantial difference between these two types of fat is that visceral fatty tissue functions as an endocrine organ, contributing to the pathogenesis of several diseases [5]. Particularly, VAT has a major impact on these diseases, and several articles underline the importance of accurately measuring visceral tissue volume [11, 28, 35]. On the other hand, there is also increased attention on body composition in which SAT and VAT determination is a critical element in addition to muscle volume measurement. Neither X-ray nor any of the nuclear medicine techniques are unable to help in precisely determining the amount of fatty tissue, only MRI and CT can provide means to segment the adipose regions in the body [9, 12, 13, 15, 18, 25]. Reviewing the literature, we found some articles that tried to estimate adipose tissue with other modalities, such as ultrasound. For example, Stolk et al. measured the distance between the peritoneum and the lumbar spine using ultrasound with a strict protocol to calculate adipose tissue volume [29] [30].

The numerical characterisation of adipose tissue volume calculated from CT data can be regarded as the most frequently used method [16, 34]. Measurement of SAT and VAT values is usually accomplished on a single CT slice at the level of the umbilicus [24] or the level of T12-L1, L2-L3, L3-L4 or L4-L5 vertebral bodies [2,

11, 13, 15, 16, 27, 35]. In theory, total volume measurement of VAT or SAT would be more advantageous than estimation from a single CT slice, however proper segmentation may not be automatically performed at the diaphragm or near the pelvis, moreover limited number of slices available at CT. Several investigators have suggested and have developed sophisticated automatic algorithms for the segmentation of adipose tissue in a large body volume [23] [31], however it has been shown recently that the single slice measurement can accurately predict the changes in VAT volume and body weight.

Today, CT is the only clinically applied imaging modality that provides quantification of the different tissues based on pixels and Hounsfield unit values. Actually, the HU scale is relative because different X-ray beam energies result in different CT values, thus, it is essential to take into consideration the applied tube voltage. Furthermore, the mentioned scale depends on the radiologists. While CT is one of the most important modalities to assess adipose volume, in the literature, several independent segmentation algorithms have been introduced applying different Hounsfield Unit (HU) ranges: −190/–30 HU, −200/–10 HU, −250/–50 HU, −195/–45 HU [5, 11, 19, 23, 24, 28, 34]. To the best of our knowledge, it has not been extensive investigation pertaining to how the HU range selection might influence the segmented SAT/VAT volumes, so we aimed to:

i) Compare three commonly used ranges

ii) Study how the selected slice position affects the segmented adipose tissue area. In addition, one of the research groups has developed a linear model to estimate the patient's body shape and BMI index along with the fat-tissue segmentation technique [10]. However, this model is rather complex, and it depends on at least six different parameters, and the actual formula varies with gender. The model also includes several arbitrary constants, depending on the CT scanner.

iii) Examine these models based on our CT data and to simplify the model.

2 Materials and Methods

Ninety-eight human CT examinations were randomly selected from March 2012 to September 2013. Since all patient related data were retrospectively analyzed, informed consent was not obtained. All CT examinations were scanned by Philips Brilliance 64 CT scanner with two different protocols. However, of the 98 participants, only 14 were tested with both protocols, where the axial length scan was shorter.

The patient population included outpatients who were being assessed for several diseases. Participants' anthropometric data: 51 males mean age of 59 years (range

31-83 years), mean weight of 87 kg (range 54-150 kg), mean height of 1.7 m (range 1.52- 1.9 m), mean body mass index 34 kg/m^2 (range 23-58 kg/m$^{2)}$) and 47 females mean age of 62 (range 32-94 years), mean weight of 75 kg (range 44-110 kg), mean height of 1.62 m (range 1.5-1.77) and mean body mass index 33 kg/m^2 (range 23-55 kg/m$^{2)}$). The local medical ethics committee approved the study and waived the requirement to obtain informed consent (DE RKEB/IKEB 6593-2023). To ensure a constant signal-to-noise ratio, a standard dose optimization algorithm was applied, in which increasing X-ray exposures were used with increasing body weight in both CT protocols. In Protocol-I, a larger mAs range was set (100-200 mAs) for better image quality, while in Protocol-II, X-ray exposures were about half of those used in Protocol-I. The tube voltage was set to 120 kV in all cases.

Three axial slices (L1 vertebra and the hilar region of the right and left kidney, respectively) [25] [26] were selected from the sagittal reconstruction for image processing. Two ROIs (region of interest) were drawn on each image manually (Figure 1) in the MATLAB program on a diagnostic monitor by a radiographer with five years of professional experience in CT imaging; the larger one was defined by the body contour (green line), and the smaller one encompassed the abdominal cavity (red line).

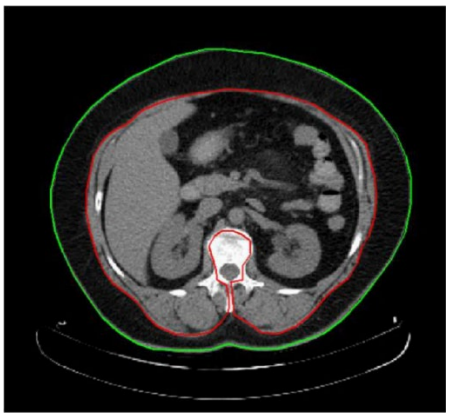

Figure 1
The amount of subcutaneous fat tissue (SAT) is defined by the total number of segmented pixels within the space between the green and red ROIs, while the visceral fat tissue (VAT) is defined by those within the region in the red ROI

Although several automatic adipose tissue segmentation algorithms are proposed in the literature [14, 23, 28, 32], they are not entirely accurate, confirmation and correction are usually necessary by radiologists. In our study, fat tissue segmentation was performed based on three different ranges of attenuation [window level/window width in HU]: -190/-30 HU, -150/-40 HU, -195/-45 [8] [31]. SAT and VAT were determined as the number of segmented pixels within the red ROI and between the red and green ROIs, respectively. Thus, SAT and VAT values were

calculated by using three different attenuation ranges. In addition, the three different SAT (SATi, i=1,2,3) and three different VAT (VATi, i=1,2,3) estimations were obtained for three different sections (Figure 2).

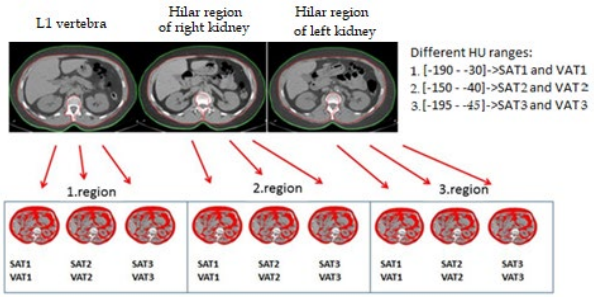

Figure 2

Segmentations were prepared with three different HU ranges using slices acquired at the level of the L.1. vertebra, and at the level of the hilum of the right and the left kidney

In each case, we calculated the BMI as follows:

$$BMI = \frac{bodyweight}{height^2}\left[\frac{kg}{m^2}\right] \tag{1}$$

The weight and height data were collected by the patients' self-declaration. Data obtained from the reconstructed images allowed us to estimate the BMI by the following formulas [8] [10]:

$$BMIest\ male: 2.069 + (0.037 \cdot SQA) - (0.05 \cdot age) + (0.984 \cdot BTD) - (2.647 \cdot L1APD) \tag{2}$$

$$BMIest\ female: -9.163 + (0.252 \cdot BC) + (10.621 \cdot \frac{SQA}{BA}) - (0.08 \cdot age) + (0.597 \cdot BAPD). \tag{3}$$

These formulas require the horizontal and anteroposterior (AP) diameters of the body (BTD, BAPD), the diameter of the vertebral body (L1APD), the body circumference (BC), the total body area (BA) of the axial slice, the subcutaneous fatty area (SQA) and the patient's age (see Figure 3).

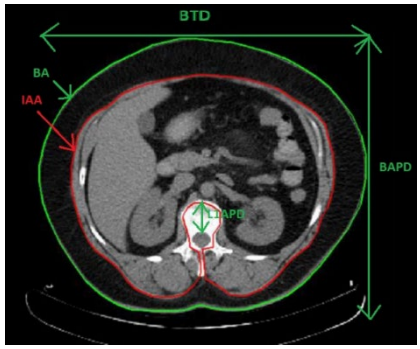

Figure 3

Different parameters for BMI estimation on an axial CT slice. The following parameters are drawn on the image: horizontal and anteroposterior diameters of the body (BTD, BAPD), the diameter of the vertebral body (L1APD), intraabdominal adipose tissue (IAA) and total body area (BA).

We thought the original model was too complex therefore, we tried to simplify it. The BMIest depends on 4-5 data, and the dependence differs for both genders. Furthermore, it is questionable whether constants depend on the actual CT setting. In the literature, we found several additional BMI models [7], and we proposed nine new models based on the original and the current models and labelled them from I to IX (see Table 1).

Table 1

Nine different models were created based on the original model for both sexes

Model numbers	**Female models**
I	BMI_{model}=-9.163+(0.252 ×BC)+ $\left(10.621\times \frac{SQA}{BA}\right)$-(0.081 ×age)+(0.597 ×BAPD)
II	BMI_{model}=a+(b ×BC)+ $\left(c\times \frac{SQA}{BA}\right)$-(d ×age)+(e ×BAPD)
III	BMI_{model}=2.069+(0.037 ×SQA)- (0.051× age)+(0.985 ×BTD)-(2.648 ×L1APD)
IV	BMI_{model}=a+(b ×SQA)- (c× age)+(d ×BTD)-(e ×L1APD)
V	BMI_{model}=a+(b ×BC)
VI	BMI_{model}=a+(b ×BTD)+ (c× BAPD)
VII	BMI_{model}=a+(b ×BC)+c ×age
VIII	BMI_{model}=a+(b ×BTD)+ (c× BAPD)+ (d ×BC)
IX	BMI_{model}=a+(b ×BTD)+ (c× BAPD)+ (c ×BC)+ (e ×age)
Model numbers	**Male models**
I	BMI_{model}=2.069+(0.037 ×SQA)- (0.051× age)+(0.985 ×BTD)-(2.648 ×L1APD)
II	BMI_{model}=a+(b ×SQA)- (c× age)+(d ×BTD)-(e ×L1APD)
III	BMI_{model}=-9.163+(0.252 ×BC)+ $\left(10.621\times \frac{SQA}{BA}\right)$-(0.081 ×age)+(0.597 ×BAPD)
IV	BMI_{model}=a+(b ×BC)+ (c×SQR)-(d ×age)+(e ×BAPD)

V	BMI_{model}=a+(b ×BC)
VI	BMI_{model}=a+(b ×BTD)+ (c× BAPD)
VII	BMI_{model}=a+(b ×BC)+c ×age
VIII	BMI_{model}=a+(b ×BTD)+ (c× BAPD)+ (d ×BC)
IX	BMI_{model}=a+(b ×BTD)+ (c× BAPD)+ (c ×BC)+ (e ×age)

We applied non-linear regression to calculate the coefficients of the nine equations where the following weight function was minimized for each case:

$$h(a,b,c,d,e) = \sum_{k=1}^{n}(BMI_k - BMImodel((a,b,c,d,e))_k)^2 \quad (4)$$

In Eq. 4, the BMI and BMImodel stand for the real and the model equation-based (presented in Table 1) BMIs, respectively. In addition, the sum runs over the whole male or female population (n_{female}= 47, n_{male}= 51).

Hypothesis tests for paired datasets were performed to compare the values obtained from different axial slices and different ranges. The distribution of the data was evaluated using the Anderson-Darling normality test. After that, the corresponding hypothesis test was chosen: paired t-test for normally distributed data and Wilcoxon signed-rank test for the rest. The datasets are considered significantly different if the p-value is smaller than 5%.

All data evaluation and processing were performed using Microsoft Office EXCEL and MATLAB, commercially available programs.

3 Results

3.1 Influence of Segmentation on SAT and VAT Values

AT data of all patients were separated according to gender, slice, X-ray exposure, type of adipose tissue, and applied range of HU during segmentation. First, we analyzed how the AT data obtained by the three segmentation methods are interrelated for gender and X-ray exposure. Figure 4 shows that the correlation coefficients are somewhat higher in the case of Protocol-I compared to Protocol-II for both subcutaneous fat and visceral fat AT data, furthermore, the correlations were independent of HU ranges.

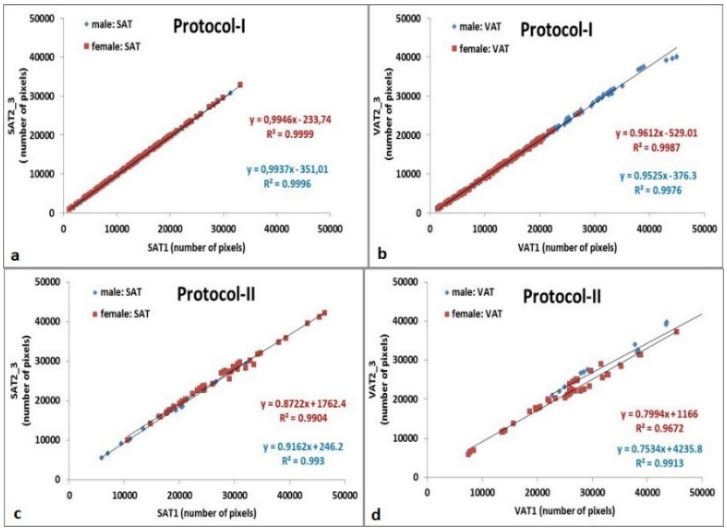

Figure 4

Correlation plots of SAT1-SAT2, SAT1-SAT3(a, c) and VAT1-VAT2, VAT1-VAT3 (b, d) for male and female subjects. Protocol-I was used in a, b and Protocol-II in c, d

The role of the protocol is understandable since Protocol-I generates more photons that may be involved in imaging. Interestingly, the correlation coefficients and the regression equations are very similar for male and female patients. Although the correlations are close, all y axis intersections differ significantly from zero. Generally, the correlation between SATi values is closer as composed to those between VATi data.

As a next step, hypothesis tests were performed to analyze how the predefined HU segmentation ranges influence the AT values obtained at different anatomical regions. Summary statistics for the hypothesis test are provided in Table 2.

Table 2

The resulting p values of the hypothesis test for paired subcutaneous and visceral adipose tissue data from different axial slices

	VAT1, VAT2	**VAT1, VAT3**	**VAT2, VAT3**
male, vertebra	5.14E-10	5.14E-10	4.17E-08
male, left kidney	5.14E-10	5.15E-10	2.66E-07
male, right kidney	5.14E-10	1.19E-28	1.31E-07
female vertebra	4.09E-28	1.46E-26	5.77E-18
female left kidney	3.31E-25	8.21E-25	7.24E-09
female right kidney	7.98E-23	1.12E-22	2.67E-15
	SAT1, SAT2	**SAT1, SAT3**	**SAT2, SAT3**

male, vertebra	5.14E-10	2.77E-30	1.45E-05
male, left kidney	5.14E-10	1.93E-30	5.24E-05
male, right kidney	5.14E-10	1.41E-29	2.41E-05
female vertebra	3.47E-26	2.33E-25	1.45E-05
female left kidney	9.13E-28	4.95E-26	5.24E-05
female right kidney	1.85E-29	8.54E-28	7.23E-13

3.2 Relation of SAT and VAT Data to Patient's Mass

The interrelationship between the number of AT pixels and the patients' weight, or BMIs was also studied. Figure 5a and 5b presents data on the correlation between AT data and patients' weight.

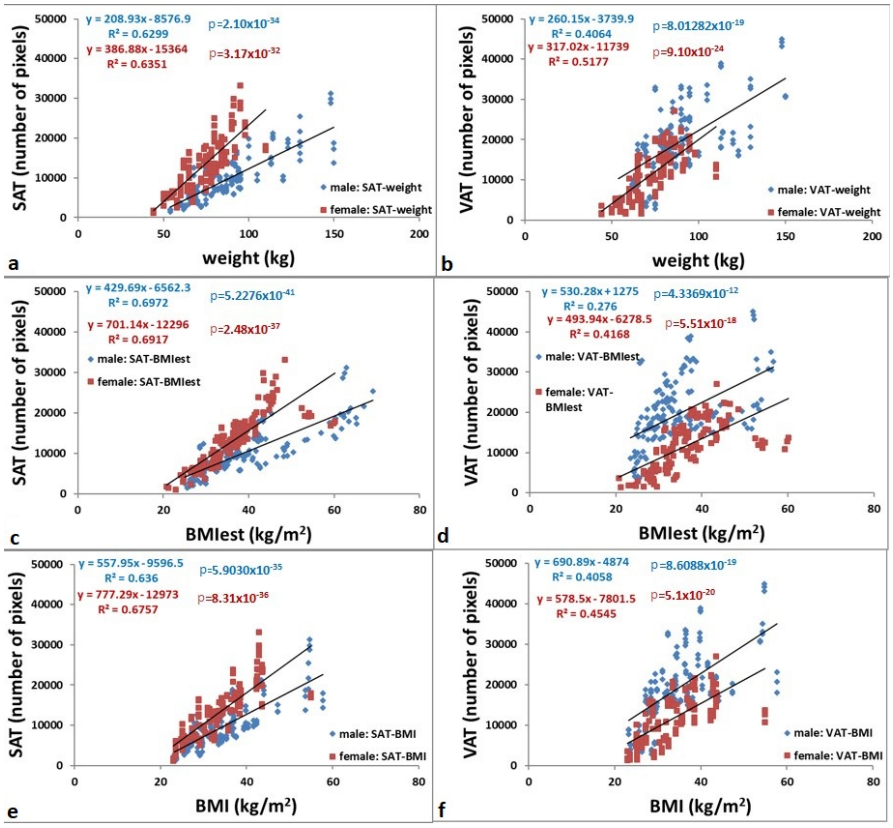

Figure 5

The interrelationship between SAT or VAT and the weight, BMIest and BMI. Adipose tissue data determined with all three HU ranges are plotted. The regression equation, the R2 and p values are shown in each plot.

As expected, the AT pixel numbers increase as a function of body weight, but the correlation coefficients are rather low, especially for visceral fat. In addition, VAT and BMIest correlations (see Figure 5d) are definitely the lowest (r^2=0.276, r^2=0.416). The only exception is the correlation between SAT and BMIest for male subjects (r^2=0.697) and female subjects (r^2=0.691, shown in Figure 5c. SAT and VAT data are better correlated with real BMI data (Figure 5e, f) being characterized by r^2 values similar to those in the correlation of AT data and real weight (Figure 5a, b). Visceral data show a significantly poorer correlation in all cases. It can also be noted that the female body contains more subcutaneous fat, whereas men have more visceral fat. This can serve as useful information since visceral fat can function as an endocrine organ and produce various hormones [16]. These hormones may damage the body in different ways.

3.3 Effect of X-Ray Exposure

Correlation analysis was performed with data obtained from the investigation of the 14 patients scanned using both protocols. The most critical difference between data using the two protocols, is the higher pixel number of the segmented adipose tissue regions yielded by Protocol-II (Figure 6).

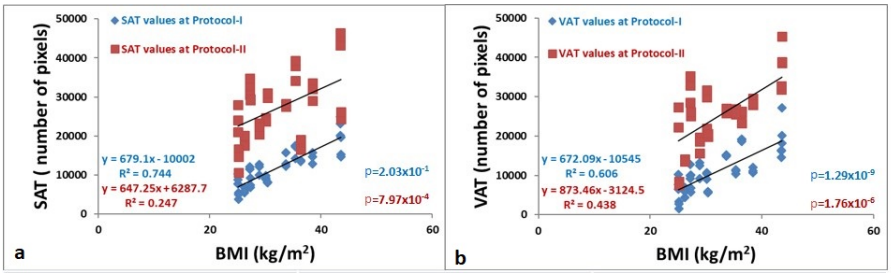

Figure 6

Interrelationship between SAT and BMI based comparison of Protocol-I and Protocol-II.
The numerical result of the regression (equation, the R^2 and p values) are presented in each graph.

The difference can be more than double. Displayed data also show a better correlation of AT data by Protocol-I with real BMI than Protocol-II, suggesting that the segmentation is more accurate if Protocol-I is applied. The correlation is high with the first protocol at real BMI (r^2=0.74 and r^2=0.606). The p value of regression analysis is almost zero (values are shown in Figure 6). Finally, it can be generally stated that the determination of subcutaneous adipose areas is more accurate with higher X-ray exposure. Plots of SAT and VAT versus body mass show an increase of adipose tissue with greater body mass, however, the interrelationship and the related correlations are less pronounced with Protocol-II (Protocol-I vs Protocol-II; SAT: r^2 = 0.745 vs 0.248 and VAT: r^2=0.606 vs 0.439).

3.4 Reliability of BMIest

Additional correlation analysis was conducted to test the reliability of the formula used to calculate BMIest. The correlation between BMIest and real BMI data is displayed in Figure 7 for both male (r^2=0.78 with p<0.001) and female patients (r^2=0.841 with p<0.001) using data obtained by Protocol-I.

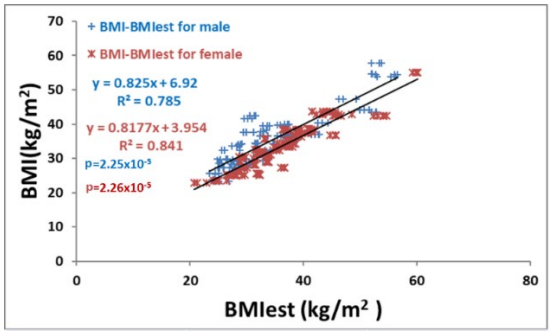

Figure 7
Correlation plot between BMI and BMIest. The resulted correlation parameters (equation, R^2 and p) are also presented.

3.5 Effect of Segmentation Levels

In the study, we also examined the segmentation differences due to the three selected regions (L.1 vertebra, left and right kidney). The results are illustrated in Figures 8 and 9. High correlations are shown at both fat tissues by the large r^2 value (Figs. 8 and 9) with a definite positive intersection at the Y axes.

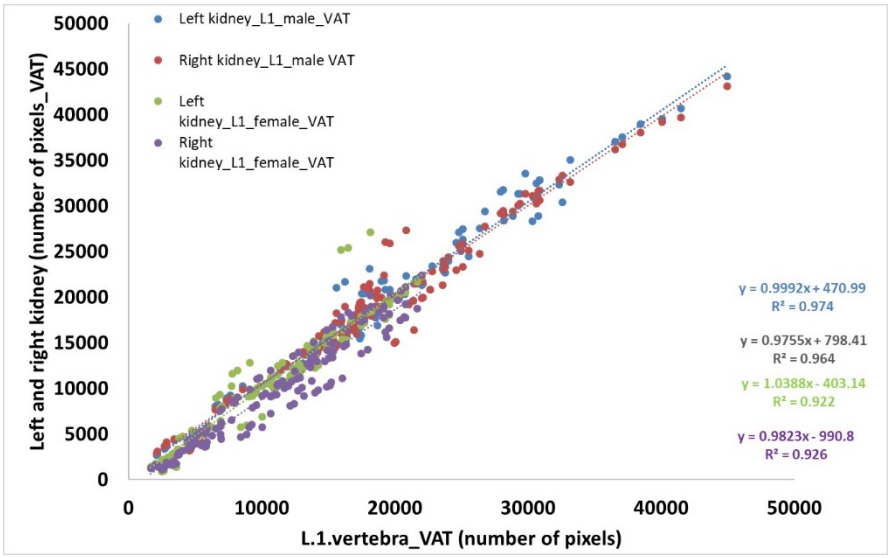

The interrelationship between the VAT values originated from the L.1vertebra and the left and the right kidney

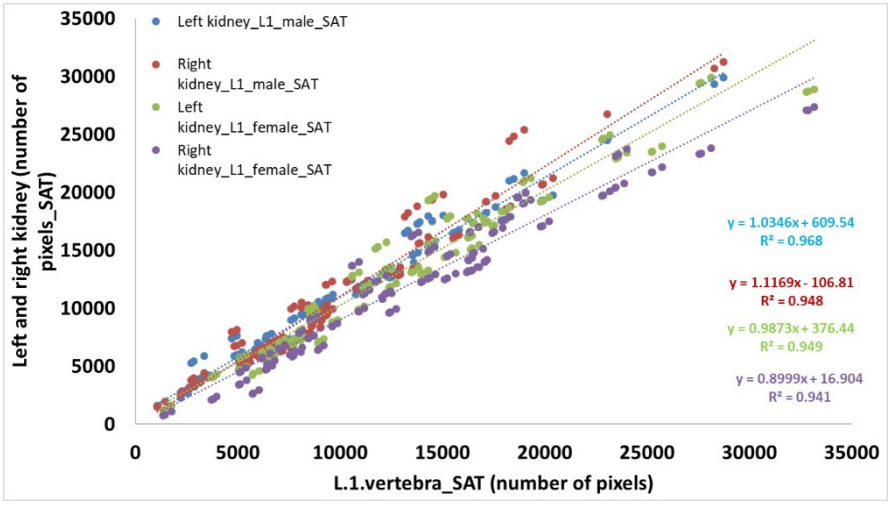

Figure 9
Correlation between the SAT values selected from L1 vertebra and left and right kidney

Hypothesis tests were also performed to compare the AT values obtained from different axial regions (Table 3).

Table 3
Summary of paired hypothesis test for subcutaneous and visceral adipose tissue data from different anatomical ranges. If p is larger than 0.05, the value is presented in red color

	vertebra, left kidney	vertebra, right kidney	left kidney, right kidney
male VAT1	1.82E-02	2.45E-02	2.69E-01
male VAT2	3.18E-02	2.19E-02	4.59E-01
male VAT3	2.83E-02	2.63E-02	3.03E-01
female, VAT1	1.33E-01	2.52E-06	2.30E-06
female, VAT2	1.74E-01	4.66E-06	4.82E-06
female, VAT3	2.05E-01	4.85E-06	3.52E-06
	vertebra, left kidney	**vertebra, right kidney**	**left kidney, right kidney**
male SAT1	7.06E-08	4.57E-06	8.52E-01
male SAT2	5.95E-08	4.18E-06	8.62E-01
male SAT3	3.75E-08	3.82E-06	8.11E-01
female, SAT1	3.66E-01	3.23E-06	2.05E-07
female, SAT2	3.48E-01	3.19E-06	1.93E-07
female, SAT3	3.52E-01	2.72E-06	1.82E-07

3.6 BMI Estimation by Models

In this section, we show the BMIs calculated by the 9 different models and then compare them. Models are shown in Table 1. The constants of models (a, b, c, d, e) are estimated by non-linear regression, and the resulting values are presented in Table 4 for men (n=51) and Table 5 for women (n=47).

Table 4
Model parameters (a, b, c, d, e) are estimated by non-linear regression, and the estimated values are presented. The h is the resulting value of the weight function used in the non-linear regression.

Male constants	*a*	*b*	*c*	*d*	*e*	*h*
Model I	2.069	0.037	0.051	0.985	2.648	125.89
Model II	-18.275	0.010	$3x10^{-5}$	1.116	-1.505	92.72
Model III	-9.163	0.253	10.621	0.081	0.597	616.80
Model IV	-0.26	0.114	$2.9x10^{-4}$	0.021	0.489	97.30
Model V	-3.22	0.249	-	-	-	103.23
Model VI	-15.799	0.911	0.395	-	-	80.46
Model VII	-3.19	0.248	$2.8x10^{-4}$	-	-	103.23
Model VIII	-12.75	0.844	$3.3x10^{-4}$	0.092	-	85.04
Model IX	-13.42	0.900	$3x10^{-4}$	0.085	-0.007	85.04

Table 5
Parameters of female models (a, b, c, d, e) are estimated by non-linear regression, and the estimated values are presented. The h stands for the resulting value of the weight function

Female constants	a	b	c	d	e	h
Model I	-9.163	0.253	10.621	0.081	0.597	390.14
Model II	-5.087	0.187	11.525	0.055	0.390	72.95
Model III	2.069	0.037	0.051	0.985	2.648	91.68
Model IV	0.110	0.014	0.045	0.953	1.114	65.26
Model V	-9.680	0.324	-	-	-	79.93
Model VI	-12.38	1.002	0.262	-	-	72.56
Model VII	-7.500	0.334	-0.060	-	-	71.23
Model VIII	-12.864	1.129	0.469	-0.082	-	71.48
Model IX	0.002	0.234	0.001	0.208	-0.069	83.65

In the last column of both tables, the value of the weight function of the non-linear regression (see Eq. 4) can also be seen. In general, the h value may depend on the number of cases and the goodness of the fitted model, thus we need to consider it when interpreting the results. Fortunately, our two groups contain almost the same number of cases, thus the h value will be comparable between the two gender groups. In the case of Table 4 the highest h value (meaning the worst model) belongs to Model III, which is the original model for the other sex (women). In this case, the h value is 616.8, approximately five times greater than Model I. The best model is Model VI, where only the AP and horizontal diameters are included. There are reduced differences among the remaining models, thus there is no need to use a complicated, multifactorial model for BMI estimation. The h values of women are in a similar range as those of men, which is probably explained by the similar number of patients in both groups (Table 5). The best h value belongs to Model IV (h=65.26) which is based on Model I of man. The worst case is Model I, which is the original model of women, and this conclusion is the same for both sexes. There are minor differences among the resting models, and especially Model VI-VIII are very close to each other because the h value differences are less than 1. Considering all models, the Model VI seems to be the most optimal for both genders because the h values are low and comprise only two distance data (BTD and BAPD).

The results of correlation analysis between the model based and real BMI are presented in Figures 10 and 11, showing the data for men and women.

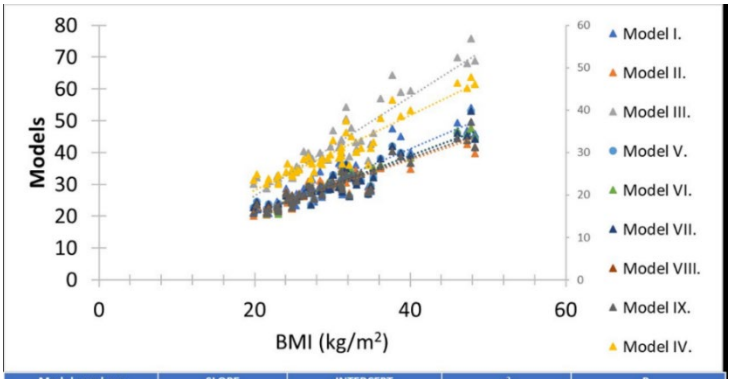

Model numbers	SLOPE	INTERCEPT	r^2	P
I.	1.043	-0.394	0.838	5.26×10^{-21}
II.	0.821	4.925	0.858	2.2×10^{-22}
III.	1.559	-4.865	0.862	9×10^{-23}
IV.	0.884	3.429	0.863	8.7×10^{-23}
V.	0.914	2.392	0.852	5.42×10^{-22}
VI.	0.923	2.218	0.899	4.51×10^{-26}
VII.	0.913	2.440	0.852	5.42×10^{-22}
VIII.	0.851	4.204	0.882	2.17×10^{-24}
IX.	0.858	3.879	0.882	2.02×10^{-24}

Figure 10
Regression analysis between BMI (kg/m^2) and models in the case of males, the regression data are in the table below the figure

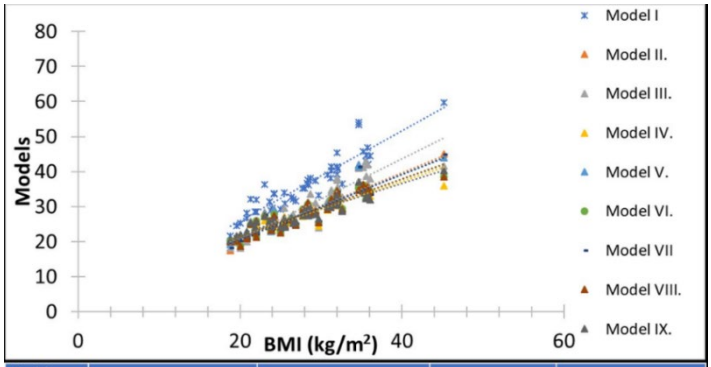

Model numbers	SLOPE	INTERCEPT	r^2	p
I.	1.282	0.341	0.852	2.86×10^{-20}
II.	0.944	1.889	0.853	2.42×10^{-20}
III.	1.147	-2.214	0.846	6.57×10^{-20}
IV.	0.785	5.773	0.867	2.66×10^{-21}
V.	0.901	3.159	0.828	8.6×10^{-19}
VI.	0.813	5.273	0.866	3×10^{-21}
VII.	0.928	2.149	0.853	2.37×10^{-20}
VIII.	0.823	4.963	0.863	4.82×10^{-21}
IX.	0.720	7.852	0.880	2.14×10^{-22}

Figure 11
Regression analysis between BMI (kg/m^2) and models in the case of females; the regression data are in the table below the figure

The points overlap in both figures. Results of regression analysis are similar in all cases because all the regression coefficients are larger than 0.8, and the ranges for women and men are 0.828-0.880 and 0.838-0.899, respectively. In addition, all correlations were significant, which is explained by the small p values (< 0.001) in the hypothesis tests.

Discussion

Determination of the amount and localization of adipose tissue plays an essential role in several diseases [20]. Several study groups have developed methods to assay tissue volume and explore the interrelationship between bariatrics and the development of defined diseases. Davies and co-workers developed an application that can successfully calculate the amount of adipose tissue in polytraumatic patients from routinely used CT scans [6]. These methods may be helpful in intensive care units for COVID-19 patients because obesity is a major risk factor and may result in a worse prognosis, mostly among young patients [4] [26]. Sala and co-workers investigated the correlation between adipose tissue distribution and cardiometabolic diseases using adipose tissue volume and distribution data obtained from CT [22]. They applied an automatic tool that could recognize fat tissue and set the Hounsfield units of fat between -150 and -30 HU and the axial slices were selected from the level of the 5th lumbar vertebra.

After the literature review, we did not find gold standard for the segmentation method. The accuracy of the segmented areas could only be verified quantitatively using phantoms, where the volume of adipose tissue or adipose tissue equivalent material in the phantom is known. Such a study was performed by Yoon et al. where they compared phantom and human CT and MR scans [9], however, in this study the main focus was the effect of varying tube current on segmentation. However, our results definitely show that image quality (influenced by the scan setup parameters), the chosen HU range and the segmentation region affect the final result. We applied the manual delineating technique and three previously published HU ranges to segment the visceral and subcutaneous areas in this study. Usually, part of the lumbal spine is the base for the adipose tissue determination, however some groups choose the level of the umbilicus [24]. In our study, adipose areas were measured on each slice acquired at the level of L1, hilar region of left and right kidney. We chose the hila of the kidneys because these are usually located between L1 and L3. The volume of subcutaneous and visceral adipose tissue was defined by these HU ranges using two different X-ray tube currents. We found that the volume of adipose tissue obtained with the higher X-ray tube current (Protocol-I) by segmentation based on different HU ranges was in good correlation ($r^2 \geq 0.998$) for both male and female subjects. Remarkable differences were detected between images and correlation analysis data applying different protocols. Images obtained with a lower (≈ 50 % lower) tube current were less reliable, and the correlations between the adipose tissue volume data segmented using different segmentation procedures were not as close as between those obtained with a larger tube current ($r^2 > 0.967$). Troschel and co-workers showed a similar tendency [3] changing the

tube current–exposure time product values in their work. In Table 2, we presented the p values for the hypothesis test, which investigated the possible effect between the segmented AT areas and predefined HU ranges at each possible region (L1 vertebra, right and left kidney level). It is visible that all p values are less than 0.05, thus it can be stated that the three different HU ranges of the segmentation affect the amount of adipose tissue segmented. This does not contradict the fact that the different AT values correlate well for each HU range, as the correlation equations' axis intercept is not zero (Fig. 4). Thus, the segmented AT values obtained with the three distinct HU ranges are not proportional to each other, only an excellent linear relationship is between them.

We were also curious about how the extent of segmented AT pixels is affected by the preselected anatomical areas (L1 vertebra, left and right kidney). The results are presented in Figures 8 and 9. Good correlations and linear relationships could be observed among each ATs, with non-zero intersections of the linear equations in every analysis. The results of the associated hypothesis tests are demonstrated in Table 3, where the p value was larger than 0.05 the text was colored in red. In the case of male and both adipose tissues, there were no significant differences between the right and left kidney level (VAT: $p>0.269$, $p>0.4591$, $p>0.303$, SAT: $p>0.852$, 0.862, 0.811), while in the case of female the vertebra and left kidney region gave same result ($p>0.133$, $p>0.174$, $p>0.205$, SAT: 0.3663, 0.348, 0.352. In all other cases, there is a difference between the segmented SAT and VAT values.

In the last step, we examined the relationship between the amount of segmented adipose tissues and the measured and estimated body shape BMI parameters. The highest correlation between segmented volume and BMIest was found with $r^2 = 0.69$ for male and female data. Comparison of the same parameters using a high and a low tube current protocol resulted in significant dissimilarities. The correlation between SAT and BMIest was characterized with $r^2 = 0.7445$ using Protocol-I and $r^2 = 0.2477$ using Protocol-II. Correlation coefficients between segmented adipose tissue and BMI or BMIest are closer if we use images obtained by the higher tube current. Studying CV data of SAT and VAT data revealed that the volume of both kinds of adipose tissue can be estimated with a $CV \leq 10$ % if the axial slice is chosen from a 5 cm wide area of the lumbal region.

CT-based determination of body mass index can be useful in two cases. One is in clinical practice, when the patient is unconscious and height and weight data are unavailable. The other is in research where no BMI or other anthropometric data are available. The latter was the case in an article by O'Leary and colleagues published in 2012. In their research, they performed adipose tissue segmentation in patients with severe acute pancreatitis without anthropometric data, so they used the BMI estimator model created by Geraghty and colleagues in 2003. In Geraghty's study, in addition to BMI, height, weight and body surface area were estimated using a single abdominal CT image.

Analyzing the nine proposed BMI models, we found that the calculated BMIest values agreed with the real BMI data (males: $r^2 = 0.7802$, females: $r^2 = 0.841$), and 7 out of the 9 models gave excellent accuracy to estimate the body shape. In addition, we found that having these seven models, the simpler ones (V, VI and VII) gave similar reliability to the original equations (I and III), so it follows that there is no need to use a complex, multifactorial model for BMI estimation.

There are some limitations to our study. First, based on the previous article, we selected the slices including the L1 [1] [8] and hila of the kidneys for adipose tissue segmentation. At the same time, other authors prefer L2-L3 or the level of umbilicus as reference [21, 24, 32]. The second limitation was the relatively few numbers of patients involved in Protocol-II. Third, we did not utilize an automatic method for segmentation, a better way could be to develop an algorithm to reduce the adipose tissue segmentation time. However, the segmentation time was not a critical aspect of our study. Finally, our study did not investigate the effects of other setting parameters on segmentation, such as the reconstruction kernel or slice thickness.

Conclusions

As three specific objectives have been identified in the introduction, we can state the following:

i) In our study, we found a good correlation between the three HU ranges, without proportionality, thus, the segmented SAT and VAT areas are actually different.

ii) The chosen anatomical level of segmentation significantly affects the VAT and SAT values.

iii) For the 98 patients, model-based BMI and real BMI were determined and compared.

We have simplified the model-based BMI estimation and as a result, we have shown that a complex multivariate model is not necessary, for CT-based BMI calculations.

Funding

Project no. TKP2021-NKTA-34 has been implemented with the support provided by the Ministry of Culture and Innovation of Hungary from the National Research, Development and Innovation Fund, financed under the TKP2021-NKTA funding scheme.

References

[1] A. A. Perez, P. J. Pickhardt, D. C.Elton et al. Fully automated CT imaging biomarkers of bone, muscle, and fat: correcting for the effect of intravenous contrast. Abdominal Radiology. 2020; 48:1229-1235

[2] A. M. Sironi, A. Gastaldelli, A. Mari et al. Visceral fat in hypertension: influence on insulin resistance and beta-cell function. Hypertension. 2004;44(2):127-33

[3] A. S. Troschel, F. M. Troschel, G. Fuchs et al. Significance of Acquisition Parameters for Adipose Tissue Segmentation on CT Images. AJR AM J Roentgenol. 2021; 217(1):177-185

[4] A. Tolonen, T. Pakarinen, A. Sassi et al. Methodology, clinical applications, and future directions of body composition analysis using computed tomography (CT) images: A review. European Journal of Radiology. 2021;145, 109943

[5] C. S. Fox, J. M. Massaro, U. Hoffmann et al. Abdominal visceral and subcutaneous adipose tissue compartments: Association with metabolic risk factors in the Framingham heart study. Circulation. 2007;116(1):39-48

[6] D. F. Ferguson, B. J. Busenlehner, M. D. Rahm et al. The Use of Routine Thoracoabdominal CT Scans in the Polytrauma Patient to Estimate Obesity. Obesity. 2013;21(5):997-1003

[7] D. M. Thomas, C. Bredlau, A. Bosy-Westphal et al. Relationships between body roundness with body fat and visceral adipose tissue emerging from a new geometrical model. Obesity. 2013;21(11):2264-71

[8] D. P. O'Leary, D. C'Neill, P. McLaughlin et al. Effects of abdominal fat distribution parameters on severity of acute pancreatitis. World Journal of Surgery. 2012;36(7):1679-85

[9] D. Y. Yoon, J. H. Moon, H. K. Kim et al. Comparison of Low-Dose CT and MR for Measurement of Intra-Abdominal Adipose Tissue: a Phantom and Human Study. Academic Radiology: 2008;62-70

[10] E. M. Geraghty, J. M. Boone. Determination of Height, Weight, Body Mass Index, and Body Surface Area with a Single Abdominal CT image. Radiology. 2003;(228):857-63

[11] H. Fang, E. Berg, X. Cheng, Wei S. How to best assess abdominal obesity. Current Opinion in Clinical Nutrition and Metabolic Care. 2018;21(5):360-5

[12] H. H. Hua, H. E. Kan. Quantitative proton MR techniques for measuring fat. NMR in Biomedicine. 2013;26(12):1609-29

[13] I. Janssen, S. B. Heymsfield, D. B. Allison et al. Body mass index and waist circumference independently contribute to the prediction of nonabdominal, abdominal subcutaneous, and visceral fat. American Journal of Clinical Nutrition. 2002;75(4):683-8

[14] J. Kullberg, A. Hedström, J. Brandberg et al. Automated analysis of liver fat, muscle and adipose tissue distribution from CT suitable for large-scale studies. Scientific reports. 2017;(November 2016):1-11

[15] J. LaForgia, J. Dollman, M. J. Dale et al. Validation of DXA body composition estimates in obese men and women. Obesity (Silver Spring).

2009;17(4):821-6, Available from: http://www.ncbi.nlm.nih.gov/pubmed/19131939

[16] J. L. Kuk, T. S. Church, S. N. Blair, R. Ross. Does measurement site for visceral and abdominal subcutaneous adipose tissue alter associations with the metabolic syndrome? Diabetes Care. 2006;29(3):679-84

[17] J. Machann, A. Horstmann, M. Born et al. Diagnostic imaging in obesity. Best Practice Research Clinical Endocrinology and Metabolism. 2013;27(2):261-77, Available from: http://dx.doi.org/10.1016/j.beem.2013.02.003

[18] J. Sun, B. Xu, J. Freeland-Graves. Automated quantification of abdominal adiposity by magnetic resonance imaging. American Journal of Human Biology. 2016;28(6):757-66

[19] K. J. Rosenquist, A. Pedley, J. M. Massaro et al. Visceral and subcutaneous fat quality and cardiometabolic risk. JACC Cardiovascular Imaging. 2013;6(7):762-71

[20] L. E. Wagenknecht, C. D. Langefeld, A. L. Scherzinger et al. Insulin sensitivity, insulin secretion, and abdominal fat: the Insulin Resistance Atherosclerosis Study (IRAS) Family Study. Diabetes. 2003;52(10):2490-6. Available from: http://diabetes.diabetesjournals.org/content/52/10/2490.full.pdf

[21] M. Hilmi, A. Jouinot, R. Burns et al. Body composition and sarcopenia: The next-generation of personalised oncology and pharmacology? Pharmacology and Therapeutics. 2019; 196:135-59, Available from: https://www.sciencedirect.com/science/article/abs/pii/S0163725818302195?via%3Dihub

[22] M. L. Sala, B. Röell, N. van der Bijl et al. Genetically determined prospect to become long-lived is associated with less abdominal fat and in particular less abdominal visceral fat in men. Age Ageing. 2015;44(4):713-7

[23] M. Nemoto, T. Yeernuer, Y. Masutani et al. Development of automatic visceral fat volume calculation software for CT volume data. Journal of Obesity. 2014: 495084

[24] M. S. Kim, Y.-J. Choi, Y. H. Lee. Visceral fat measured by computed tomography and the risk of breast cancer. Translation Cancer Research. 2019;8(2):1939-49

[25] M. S. Middleton, W. Haufe, J. Hooker et al. Quantifying Abdominal Adipose Tissue and Thigh Muscle Volume and Hepatic Proton Density Fat Fraction: Repeatability and Accuracy of an MR Imaging-based, Semiautomated Analysis Method. Radiology. 2017;283(2):438-49, Available from: http://pubs.rsna.org/doi/10.1148/radiol.2017160606

[26] M. Watanabe, D. Caruso, D. Tuccinardi et al. Visceral fat shows the strongest association with the need of intensive care in patients with COVID-19, Metabolism. 2020; 111:154319

[27] N. Linder, S. Michel, T. Eggebrecht et al. Estimation of abdominal subcutaneous fat volume of obese adults from single-slice MRI data – Regression coefficients and agreement. European Journal of Radiology. 2020;130(December 2019):1-7

[28] P. Decazes, A. Rouquette, A. Chetrit et al. Automatic Measurement of the Total Visceral Adipose Tissue from Compute Tomography Images by Using a Multi-Atlas Segmentation Method. Journal of Computer Assisted Tomography. 2018;42(1):139-45

[29] R. L. R. Novais, A. C. C. Café ,A. A. Morais et al. Intra-abdominal fat measurement by ultrasonography: association with anthropometry and metabolic syndrome in adolescents. Jornal Pediatria (Rio J). 2019;95(3):342-9, Available from: https://doi.org/10.1016/j.jped.2018.03.004

[30] R. P. Stolk, O. Wink, P. M. J. Zelissen et al. Validity and reproducibility of ultrasonography for the measurement of intra-abdominal adipose tissue. International Journal of Obesity. 2001;25(9):1346-51

[31] S. Cecchini, E. Cavazzini, F. Marchesi et al. Computed tomography volumetric fat parameters versus body mass index for predicting short-term outcomes of colon surgery. World Journal of Surgery. 2011;35(2):415-23

[32] S. J Lee, J. Liu, J. Yao al. Fully automated segmentation and quantification of visceral and subcutaneous fat at abdominal CT: application to a longitudinal adult screening cohort. British Journal of Radiology. 2018;(March):4-9

[33] S. M. Grundy., I. J. Neeland, A. T. Turer, G. L. Vega. Waist Circumference as Measure of Abdominal Fat Compartments, J Obesity, J Obes [Internet] 2013; e454285, Available from: http://www.hindawi.com/journals/jobe/2013/454285/abs/

[34] W. O. Grauer, A. A. Moss, C. E. Cann, H. I. Goldberg. Quantification of body fat distribution in the abdomen using computed tomography. The American Journal of Clinical Nutrition. 1984;39(4):631-7

[35] X. Cheng, Y. Zhang, C. Wang et al. The optimal anatomic site for a single slice to estimate the total volume of visceral adipose tissue by using the quantitative computed tomography (QCT) in Chinese population. European Journal Clinical Nutrition. 2018;72(11):1567-75